Influence of two APS coatings on the high-speed tribological behavior of a contact between titanium alloys

Mathieu Marquer, Sylvain Philippon, Laurent Faure, Guillaume Chassaing, Joffrey Tardelli, Karim Demmou

Influence of two APS coatings on the high-speed tribological behavior of a contact between titanium alloys

Mathieu Marquer[a,b], Sylvain Philippon[a], Laurent Faure[a], Guillaume Chassaing[a,*], Joffrey Tardelli[b], Karim Demmou[c]

a. Université de Lorraine, CNRS, Arts et Métiers ParisTech, LEM3, F-57000 Metz, France
ENIM – Laboratoire LEM3, 1 route d'Ars Laquenexy, 57078 Metz Cedex 03, France
b. IRT M2P
Bâtiment CIRAM, 4 rue Augustin Fresnel, 57070 Metz, France
c. Safran Aircraft Engines
Rond Point René Ravaud – Réau, 77550 Moissy-Cramayel, France

* Current address: Institut de Soudure, Plateforme Mécanique-Corrosion, Espace Cormontaigne, 4 bd Henri Becquerel, 57970 Yutz, France

Corresponding author:

Sylvain Philippon

Address: ENIM – Laboratoire LEM3
1 route d'Ars Laquenexy
57078 Metz Cedex 03
France

Tel: +33 (0)3 72 74 86 54

Fax: +33 (0)3 72 74 86 12

Email: sylvain.philippon@univ-lorraine.fr

Abstract

Contacts between titanium alloys may use an anti-fretting coating on one component. However violent events may cause severe sliding.

In the high speed and pressure (up to 60 m/s and 280 MPa) sliding of a non-coated on a coated part, we investigate the influence of the coating (CoCrAlYSiBN or CuNiIn) on the friction coefficient, wear, and microstructural affectations. Both coatings did not significantly influence the friction coefficient but reduced the wear.

A scenario based on interface-localized heat explaining the generation of a third body and its influence on the tribological behavior was proposed. The dependence of the mechanical and thermal affectations on the coating material was explained based on the kinetic of the α→β phase transformation of the Ti6Al4V alloy.

Keywords

Dry friction; High-speed; Thermally-sprayed coating; Scanning electron microscopy.

1 Introduction

Titanium alloys show a good compromise between density, strength, resistance to corrosion and operating temperature. Since it became possible to mass produce them in the 1950's [1], titanium and its alloys have been increasingly used in a lot of assemblies, and with 60% of the total production, Ti6Al4V is the most popular titanium alloy [2]. In jet engines, the poor tribological properties of titanium alloys [3] especially evident in cases of fretting solicitations [4,5], led to the creation of specific coatings, such as CuNiIn and CoCrAlYSiBN, used at the blade root / disk slot contact. While these coatings play their protective role in fretting conditions [6–11], their tribological behavior, when subjected to other kinds of solicitations is however usually unknown. Aircraft engines can undergo violent events, such as bird ingestion, leading to severe loading of the blade root / disk slot contact. Its behavior in the severe (high speed and pressure) dry sliding conditions thus created may greatly influence the response of both contacting parts to the event, as well as the maintenance procedures and costs.

The friction coefficient μ is defined by the Amontons/Coulomb law as the ratio of the friction force F_T to the normal force F_N. It has been shown that above a critical sliding speed (e.g. $1\ m/s$ for a steel-on-steel contact, according to Lim *et al.* [12]), the friction coefficient, while dependent on the "true contact area" during the contact [13–17], is relatively independent from the initial roughness of the components [12]. It is mainly influenced by sliding parameters: in this study, the sliding speed v and the apparent contact pressure $p = F_N/S$, where S is the apparent contact area [12,18–24].

In severe friction, the mechanical energy dissipated in the contact is mostly converted into heat [25], even though no consensus has been found on the exact dissipation site [26–28]. The resulting surface temperature may reach high levels [14,29–31] (i.e. $1050°C$ for a steel-on-steel steel contact at $7\ m/s$ and $1.33\ MPa$ [14] and $1000°C$ for a Ti6Al4V-on-GCr15 steel

contact at 60 m/s and 1.33 MPa [31]) and has been shown to be linked to the activation of specific wear mechanisms such as adhesion or melting [12,30,32–34]. In high-speed friction, the main wear mechanism involved is generally considered to be the shearing of the adhesive junctions between the surfaces, although melting may occur in the most severe conditions [17,20,32,35].

Depending on the temperatures reached, the microstructure of Ti6Al4V may evolve and so may the mechanical properties of the alloy. At room temperature, the biphasic Ti6Al4V alloy is constituted of a HCP lattice α-phase and a BCC lattice β-phase. When the temperature is higher than its β-transus temperature (from 950°C to 1000°C depending on the source, e.g. 956°C [36], 975°C [37], 1000°C [38]), the alloy is only constituted of β-phase.

The microstructure of the parts has been shown to be modified by the severe friction. In the case of short distance contacts in severe sliding such as the ones studied in this paper, the works of Chassaing *et al.* [30,34,39] for a Ti6Al4V-on-Ti6Al4V contact revealed the formation of multiple layers in the microstructure of the parts. They investigated friction, in severe conditions ($p \approx 110$ MPa, $40\ \mathrm{m/s} \leq v \leq 64\ \mathrm{m/s}$), of a longer, moving part, in linear sliding against a shorter, fixed one, both made of non-coated Ti6Al4V. They highlighted the key mechanisms of this interaction. Firstly, the microstructure exhibits a highly strained layer and heat-affected zone in both parts. Furthermore, the wear mechanism is adhesive, a transfer of material being observed from the fixed body to the moving one. This transferred material forms a third body which reduces the friction coefficient during the interaction. A time dependent behavior scenario was proposed which explains the behavior of the non-coated Ti6Al4V contact in severe friction. It is based on heat accumulation in the shortest part. This leads to the thermal softening of the surface of this component, reducing the friction coefficient but at the cost of a significant wear of the smaller part. This heat buildup has been confirmed by thermal measurements, with contact temperature reaching 1400°C [30]. These

results will serve as a reference for comparing the behavior of anti-fretting coated titanium alloy sliding against a non-coated titanium alloy. However, since all studies about the friction of these coatings have been made with fretting solicitations [8–11], their tribological behavior under severe conditions had to be investigated first.

The aim of this work is thus to investigate the effect of the presence of two anti-fretting coatings, namely CuNiIn and CoCrAlYSiBN, on the tribological behavior of the dry contact between Ti6Al4V alloys in the specific conditions of severe friction. CuNiIn is usually used as a supporting layer for an MoS_2 solid lubricant but for this study we considered it to have worn out under fretting solicitations prior to the interaction. This work is focused on sliding speeds ranging from 40 m/s to 60 m/s for apparent contact pressures of 110 MPa and 280 MPa. These values were chosen in order to get testing conditions as close as possible to the ones used for the Ti6Al4V-on-Ti6Al4V contact [30,34,39] and to real loading conditions [34,40]. The effect of the coating material, sliding speed and apparent pressure on the friction coefficient and wear volume were studied. In addition, the influence of the coating material on the microstructural alteration of the samples was investigated. The results were then compared to those from a contact without coating from literature [30,34,39]. From these observations, for this contact, a tribological behavior scenario which takes accounts of the main characteristics of the solicitation has been proposed. Based on this scenario the local shear stress and heat flux were then calculated and compared to the sheared and heat-affected depths of the longer, non-coated, sample. The role played by the third body in the microstructural alterations of the moving sample was discussed.

2 Materials and methods

2.1 Experimental setup

Several kinds of devices are available for tribological studies, depending on the test conditions considered. In this work, the main constraints were the sliding speed ($40\ m/s <$

$v < 60\ m/s$) and apparent pressure ($110\ \text{MPa} < p < 280\ \text{MPa}$) ranges. Criteria also included a moderate (less than 100 mm) but not too short (more than 1 mm) sliding distance and a quasi-absence of running-in period. The well-known pin-on-disc tribometer needs multiple rotations in order to reach high speeds, modifying both contact surfaces during that time. It could thus not be used. After considering various other devices, such as the plate impact [22] and Ogawa's modification of the Kolsky bars [39], a slider-on-pad setup was adopted.

The slider-on-pad tribometer was first designed by Philippon *et al.* [23,42] and was later successively enhanced. In this work, the third version of this device, adapted to a ballistic bench, is employed. This configuration is detailed in reference [34]. For each experiment, a set of three specimens was used: one slider and two pads. After placing the slider of length L_S in-between the pads of length L_P (see Fig. 1), the normal force is applied on the stack by a dynamometer ring. The slider is impacted by a projectile, causing it to accelerate in less than 50 µs [43] to a speed called "initial sliding speed" v_i. During the experiment, the normal force F_N imposed by the dynamometer ring and both tangential forces F_{T1} and F_{T2} resulting from the friction on each pad are recorded. An average friction force F_T is calculated from the two latter.

The interaction can be divided into 3 main stages which are highlighted in Figs. 1 and 2. At the beginning (phase 1), the projectile impacts the slider which starts moving. The inertia effects cause a peak of tangential force. After this transient period, the system is in a relatively steady state (phase 2), qualified by a variation of F_T within ±30%. When the end of the slider reaches the pads ($t = v.(L_S - L_P)$), the contact area decreases, causing the apparent contact pressure to increase. This is the beginning of third phase, which ends when the slider is no longer in contact with the pads ($t = v.L_S$).

Given the nature of phases 1 and 3, only the second phase is considered for calculating the friction coefficient. From the normal and average friction forces, a coefficient of friction $\mu(t) = F_T(t)/F_N(t)$ is calculated. The average value $\bar{\mu}$ is used as the test friction coefficient.

2.2 Materials

For this study, both sliders and pads were machined by milling from a Ti6Al4V alloy (90 % Ti + 6 % Al + 4 % V) whose microstructure is shown in Fig. 3.a. The characteristic dimensions of the specimens (represented in Fig. 1) were $L_S = 60\ mm$, $L_P = 10\ mm$ and $l_S = 3\ mm$, so the apparent contact area was $S = L_P * l_S = 30\ mm^2$. The pads were coated of either CuNiIn or CoCrAlYSiBN by air plasma spraying (APS). The powders used for this operation had the following compositions, given as mass fractions. The CuNiIn coating was obtained from a single powder, consisting of 59 % Cu + 36 % Ni + 5 % In. The CoCrAlYSiBN coating was obtained from a mix of two components: 75 % of a powder of a CoCrAlYSi alloy (composition: 52.98 % Co+ 25 % Cr + 8.47 % N + 6.53 % B + 5 % Al + 1.75 % Si + 0.27 % Y) and 25 % of a hexagonal boron nitride (56.5 % N + 43.5 % B) one. A cross-section of the coatings (Figs. 3.b and 3.c) shows the resulting microstructures. The CuNiIn coating (thickness: $e_{CuNiIn} = 160\ \mu m$) is mainly composed of CuNiIn grains, but also includes various oxides and porosity created during the spraying process. The CoCrAlYSiBN coating (thickness: $e_{CoCrAlYSiBN} = 180\ \mu m$) also includes oxides and porosity but is mainly composed of two phases: a CoCrAlYSi matrix and hexagonal boron nitride inclusions. These inclusions, aimed at providing the contact with a solid lubricant through the life of the coating, represent 25 % to 30 % of the coating volume. The manufacturer, using image analysis on optical micrographs (details of the method are confidential), measured the typical initial porosity volume fraction to be close to 2 % for both coatings.

The initial roughness ($Ra_{Ti6Al4V} \leq 0.4$ µm, $Ra_{Coatings} \leq 6$ µm) is not considered to be a critical parameter when considering the high-speed friction behavior of a dry contact. The

range of sliding speeds studied in this work allows to not investigate the influence and evolution of roughness.

2.3 Post-mortem characterization

After the friction tests, the slider, projectile, and pads were retrieved in a receiving tank filled with shock absorbing material (cloth) in order to dissipate the kinetic energy of the parts. The samples were then characterized by two successive methods. The wear was firstly measured, after which SEM observations of the parts were performed.

2.3.1 Apparent wear volume measurement

The wear can be measured either as a mass or a volume variation. While measuring mass variation is certainly easier than any other method, this technique requires to be able to ascertain that no mass variation happens outside the friction test itself. With the setup of these experiments, it was not possible. The projectile may impact the slider in the receiving tank while shock absorbing material may become glued to the slider. The pads, sucked in the receiving tank by the trail of the projectile, may also suffer post-test mass variation for reasons similar to the sliders. This only enables the wear measurement by a volumetric method.

The apparent wear volume was measured by using a focus variation microscope (Alicona Infinite Focus) which acquired the part topography. A 5x objective was used, giving the system a lateral resolution of 10 µm and a vertical one of 0.50 µm. It was possible to compute the wear volume of the part by comparison of the measured topography with a reference surface defined on a non-worn surface. While damage to parts of the samples remote from the friction zone may influence the results from mass variation or total volume methods, this technique allows to consider only the wear scar area during the volume measurement.

On the pads, the reference surface was defined as the mean plane of the non-worn surface present on each side of the wear scar. On the sliders, however, no reference surface was available. Since no method was suitable for the measurement of the wear of the sliders, the wear volumes were only studied for the pads. For a friction test, the wear volume w is the mean value of the apparent wear of the two pads.

Due to the porous microstructure of the coatings, it should be noted that the very high apparent contact pressure may cause these materials to be subjected to densification (i.e. closing of the pores) before the beginning of the interaction. This may increase the measured apparent wear volume, and thus cause an overestimation of its value. The small initial porosity fractions (about 2 % for both coatings), is however unlikely to cause a significant overestimation of the wear volume.

2.3.2 Microstructural analysis

The pads and sliders surfaces and sections were observed by means of an SEM (Zeiss Supra 40 SEM-FEG). The positions of the observed zones are represented in Fig. 4. The SEM was equipped with a secondary and a backscattered electron detectors as well as an energy dispersive X-ray spectrometer for chemical analysis (EDX analysis). This detector was used to qualitatively assess the presence and determine the main components of transferred materials.

Observing the surfaces of the samples only required a degreasing step, which consisted of an ultrasound cleaning in an acetone-ethanol mix (50 vol% of acetone). For the sections, however, the observed surface needed a polishing step beforehand. A semi-automatic polishing machine (Struers Tegramin-20) was used for all polishing steps. Coarse polishing was done using SiC sandpaper down to a 15 µm grain size, followed by fine polishing using 9 µm and 3 µm diamond polishing suspensions. The last polishing step involved hydrogen peroxide-activated OPU.

3 Results and discussions

The sliding tests were carried out at three target initial sliding speeds ($v = 40, 50$ and $60\ \mathrm{m/s}$) under two target apparent contact pressure values ($p = 110$ and $280\ \mathrm{MPa}$).

The test configurations only differ from each other by the nature of the coating used on the pads, while the slider and the pads substrate material is always the same (Ti6Al4V). For the sake of readability, the test configurations used hereinafter are designated using shortened names “cM”. In this notation, “M” is the abbreviated name of the material present on the surface of the pads (Co and Cu respectively for the CoCrAlYSiBN and CuNiIn coatings).

3.1 Friction coefficient value and wear volume

From these tests, the average friction coefficients were calculated (with a 95 % confidence interval within $\bar{\mu} \pm 5\ \%$). These results (Fig. 5) highlight similar values of the friction coefficients resulting from tests performed at the same apparent contact pressure. For both couples of materials, the friction coefficient dependency to the sliding speed was low while the influence of the apparent contact pressure was more significant. An increase of the pressure of close to 150 % nearly halved the friction coefficient (from $\bar{\mu} \approx 0.15$ for $p = 110\ \mathrm{MPa}$ to $\bar{\mu} \approx 0.08$ for $p = 280\ \mathrm{MPa}$).

The apparent wear volumes of the pads were measured for a reduced set of tests. As explained in Section 2.3.1, the value used to represent a test is the average of the wear volume of both pads. The results are reported in Fig. 6. For a constant apparent normal pressure, the coated pads wear exhibits a low sensitivity to the sliding speed, regardless of the coating material, for the range of sliding speeds studied. For both couples of materials, the rise in the initial apparent contact pressure increased the wear volume. At 40 m/s, the variation is close to $0.1\ mm^3$ with both coatings materials. At higher speeds, however, the influence of the pressure appears to decrease. Indeed, at 60 m/s, the wear volumes are nearly identical for both apparent contact pressures.

At $v = 40$ m/s and $p = 280$ MPa, slight differences of friction coefficient and wear volume were observed between the two configurations. In the cCo configuration ($\bar{\mu} \approx 0.091$ and $w \approx 0.24$ mm^3), the friction coefficient and the wear volume were higher than in the cCu one ($\bar{\mu} \approx 0.063$ and $w \approx 0.19$ mm^3) by about 0.03 and 0.05 mm^3, respectively.

3.2 Evolution of the microstructure

The microstructural observations of the samples from a given couple of materials revealed similar microstructures for all pads and similar microstructures for all sliders. The microstructure remained mostly unchanged (i.e. similar thickness of the sub layers) along the length of each slider. The evolution of the microstructure along the length of the slider is a marker of the temporal evolution of the contact conditions. These were thus considered to have been stationary for the duration of the sliding test. For different sliding speeds and contact pressures, the observed evolution of the microstructure (morphologies, layering…) were similar for a given couple of materials. Therefore each test configuration is not detailed here and figures only show samples from tests at $v = 40$ m/s and $p = 110$ MPa as a case study.

A large part of the contact surface of the coated pads (Fig. 7) was found to be covered with a layer of material which presented a number of unoriented cracks. This type of cracking is typical of a relaxation of isotropic plane stress due to thermal shock from very high cooling rates [44]. This means that the contact interface reached a relatively high temperature, which is consistent with the high energy dissipated into the contact. The repartition of this layer on the surface of the pad is illustrated by Fig. 8, with micrographs corresponding to a cCu configuration. At the front of the pad, the deposited layer is absent, while it covers the rest of the friction scar. The transition between those two surfaces happens at a distance L^{act} from the front edge of the pad, called the deposit activation length. At 40 m/s and 110 MPa, in the

illustrated cCu configuration, the transition took place at $L_{cCu}^{act} \approx 5$ mm while it was 2 mm $\leq L_{cCo}^{act} \leq 3$ mm with cCo.

A layer of deposited material was also found on the whole contact surfaces of the sliders. While some cracks could be observed in the deposited layer on the sliders from the cCo tests (Fig. 9.a), few to no cracks were seen at the surface of the sliders from the cCu tests (Fig. 9.b). EDX analysis (see EDX spectra of the deposited layer in the cCu and cCo configurations in Fig. 10) revealed elements from both the Ti6Al4V alloy and the tested coating, whether in the case of the samples from the cCo or cCu tests. The relative composition of the deposited layer was estimated to be mostly Ti6Al4V in addition to some coating material. This means that the layer originates from the mix of these materials. The deposited layer from the cCu tests, however, seemed to contain a little more coating material than the one from the cCo tests.

The formation of a third body, originating mostly from the slider, during the friction was thus highlighted.

The observation of the cross-section of the sliders from the cCo tests (Fig. 11.a) revealed that the slider was layered in 4 distinct zones. The bulk of the slider (1) is unaffected by the friction process. A sheared zone (2) appears from 10 µm under the surface, while a thinner (5 µm thick) heat affected zone or HAZ (3) overlaps it up to the surface. A fourth layer of deposited material is present over the surface of the slider (4). The thickness of this layer has no meaning. Indeed, it may have been altered by the shock that took place after the interaction. It was therefore not measured. The observation of the cross-section of the sliders from the cCu tests (Fig. 11.b) reveals that they had been layered in the same four zones as the cCo sliders. The heat affected zone was however thicker (around 10 µm) than the sheared zone (5 to 7 µm). The HAZ was revealed by the presence of an acicular α' microstructure. This structure appears when the material is quenched under high cooling rate from β structure (temperature higher than the β-transus). The sheared zone was visible thanks to the typical

aspect of the β grains which appear to have been "dragged" along the sliding direction by the friction process.

A layer of deposited material is also present on the surface of the pads from both the cCo and cCu tests but no heat affected or sheared zone is revealed by the observation of their cross-section (Figs. 11.c and d). This fourth layer was also visible in the observations of the surface of the samples. It has been demonstrated that this deposit originates from a third body formed of the materials of both parts during the friction.

A section of the third body deposited in valleys of the pad roughness is presented in Fig. 12 and reveals a fine structure of this layer. Submicronic heterogeneities are present in both configurations, leading us to consider the third body to originate from an accumulation of very small debris, compacted and mixed into a third body. Given the resolution of EDX analysis (about 1 µm in our case) and the small size of the debris (<0.5 µm), it was not possible to analyze their chemical composition so only the macroscopic composition, presented in the previous section is available.

The morphology of the third body deposit present on the slider (Fig. 9), and the presence of said third body on both first bodies leads us to believe severe shearing happened within a layer of third body present between the first bodies (S3M3 mode [45,46]). The morphology of the Ti6Al4V slider revealed under the third body, especially visible in Fig. 9.b, doesn't exhibit much visible damage. This leads us to postulate that the third body had a protective role in the contact by localizing the speed accommodation.

From the repartition of the third body along the pad, we showed that its formation activated only after a certain distance L^{act}. Furthermore, we showed that the slider exhibited a highly strained layer that would be characteristic of a S1M1 (superficial creep) accommodation mode. Given the role of the third body it is probable that this mode is only active prior to third body formation, that is, before L^{act}. In order for the third body to form,

some sort of threshold must be reached, as shown by the existence of the third body activation length. The existence of a heat affected zone in the slider led us to conclude that a high interfacial temperature had been reached during the contact. Furthermore, given observations made in similar loading cases by other authors (e.g. [30]), this threshold could be of a thermal nature such as reaching a temperature where shearing yield strength of the material of one of the first bodies is lowered below the frictional shear stress applied at that point of the contact.

It should be noted that, from the micrographs of the cross-section of the pads (Figs. 11.c and d), the integrity of both coatings was preserved with no severe wear mode (e.g. spalling or delamination) being activated.

Another point of interest is the EDX analysis of the third body of cCo and cCu tests (Fig. 10) revealed that the third body from cCo tests seemed to contain a little more Ti6Al4V (and conversely a little less coating material) than the one from cCu tests. The third body from cCo tests was also constituted of bigger debris than the one from the cCu tests. Indeed, from Fig. 12 the larger debris from the cCo third body (1.7 µm) were about twice as big as the larger debris from the cCu third body (0.7 µm). We saw that at $v = 40$ m/s and $p = 280$ MPa, the friction coefficient and the wear volume were slightly higher in the cCo configuration than in the cCu one (Section 3.1). This could indicate that the CuNiIn coating was more easily worn than the CoCrAlYSiBN one, leading to the formation of smaller particles under lower stresses. This would have led to the lower rate of Ti6Al4V observed in the third body generated in cCu tests, relative to the one from cCo tests.

3.3 Comparison of the experimental results to the non-coated case

In the previous section, we saw how a severe contact between a Ti6Al4V slider and coated Ti6Al4V pads behaved in terms of friction coefficient, wear volume and microstructural alterations with two different coatings (CoCrAlYSiBN and CuNiIn). Chassaing *et al.* [30,34,39] studied the contact between a Ti6Al4V slider and Ti6Al4V pad with a similar

experimental setup. Their works were used as a reference of a contact with non-coated pads. Any result for this configuration, designated as “cNC” (for non-coated), further encountered in the present paper will refer to these works.

The friction coefficient values observed were similar with both coatings (see Section 3.1). The results from the cNC configuration also exhibited the same tendency, with values close to the ones from the cCo and cCu tests (Fig. 5). Thus, all three configurations showed little sensitivity to the sliding speed but were significantly influenced by the apparent contact pressure value.

These similar behaviors may originate from the activation of similar friction mechanisms. An explanation for the observed values would be the thermal softening of the surface of at least one of the solids, caused by the quick elevation of the temperature of the contact interface. The friction power being mostly dissipated as a heat flux, the interface can reach very high temperatures, which causes the yield strength of the materials to drop and thus the friction coefficient to decrease. This phenomenon was already observed in the case of a contact between a Ti6Al4V slider and a Ti6Al4V pad by Chassaing *et al.* [30]. It was caused by the high interfacial temperature reached during the friction. For sliding speeds of 45 and 60 m/s (with $p = 110\ MPa$), the temperature was measured to be close to 1400°C in both cases.

If thermal softening took place during the tests done with coated pads, the affectation of the microstructure should testify of the high temperature necessary for the process. This aspect was discussed in Section 3.2.

For a constant apparent normal pressure, the coated pads wear exhibits a low sensitivity to the sliding speed, regardless of the coating material, for the range of sliding speeds studied. This behavior is different from the one observed in the cNC configuration (Fig. 6). In this case, the results show a sharp decrease in the apparent wear with an increase in speed. The values of the cNC, cCo, and cCu configurations tend to converge at 60 m/s, with values between 0.15

mm^3 and 0.2 mm^3. At lower speeds, however, the wear values from the cNC configuration are much higher than those from both cCo and cCu. At 40 m/s, a difference of $0.5\ mm^3$ to $0.6\ mm^3$ is observed.

For both couples of materials, the rise in the initial apparent contact pressure increased the wear volume. The increase was higher for the cNC configuration (around $0{,}3\ mm^3$ at 40 m/s) than for the cCo and cCu ones (around $0.1\ mm^3$ at 40 m/s). The apparent contact pressure had a lower influence on the wear volume at higher speeds than at lower ones. Indeed, at the highest sliding speed (60 m/s), the wear volumes are nearly identical for both apparent contact pressures.

These observations show that even though at 60 m/s the wear of the non-coated material couple is similar to the wear of the couples with the coated pads, over the rest of the speed and pressure ranges that have been studied, the coating provides a wear protection to the pad for a 60 mm sliding length. It should be noted that the wear reduction caused by the use of the coatings was not correlated, either positively or negatively, with an evolution of the friction coefficient.

The microstructural observations of the samples from a given couple of materials revealed similar microstructures for all pads and similar microstructures for all sliders (Section 3.2).

The sliders microstructures were layered in the same four zones for the three configurations, however, the thickness of the sheared and heat affected zones depended on the configuration. The composition of the deposited material was also different for the three configurations. In the case of cNC, it originated mostly from the pad while with cCo and cCu it was a mix of Ti6Al4V from the slider and of the coating material.

The microstructure of the pads was also observed. While no heat affected or sheared zones was seen in the coatings, it was observed that the deposit covered a large part of the surface.

3.4 Behavior scenario

From the microstructural observations, the activation of multiple tribological mechanisms can be deduced. A tribological behavior scenario is proposed in Fig. 13 to explain their roles and their activation points. Since the slider alterations were observed on most of the slider length, this scenario is based on the hypothesis of stationary conditions quickly established at the beginning of the friction. It describes the succession of phenomena that are activated at a point of the slider going through the contact.

1. When it enters the contact, a point of the slider surface goes through a phase of plastic deformation. Since significant friction stresses exist between the pad and slider materials, both surfaces tend to suffer from severe shearing. The repartition of the shearing deformation among the surfaces in contact depends on the shearing yield strength of the materials.
2. The mechanical energy is dissipated in the contact as heat. Its build up causes a quick temperature increase at the contact interface.
3. When the temperature reaches a high enough value, the surfaces of the samples start to soften. A third body is thus formed and maintained throughout the rest of the contact. It lubricates the contact, reducing the local friction coefficient and the wear. This third body may originate from any or both of the materials depending on their thermomechanical properties.
4. When the slider surface element exits from the contact, it is quickly cooled from its high temperature, and thus quenched (if the slider material can be transformed by quenching). This is the case of the Ti6Al4V and of most other metals. Cracking of the surface may appear due to its very high cooling rate.

This behavior scenario highlights the tribological mechanisms activated during the sliding of the components. However, in order for it to be valid, the observations of all the different

coatings studied had to be consistent with each other. From the activation length and the coefficient of friction, thermal and mechanical loads were predicted. They were compared to the measured microstructural alterations in order to check that the results from the three configurations (cCo, cCu, and cNC), were consistent.

The results from an experiment ran at a $v = 40$ m/s sliding speed and a $p = 110$ MPa apparent contact pressure were compared (Tab. 1). Under these conditions, the mean friction coefficients $\bar{\mu}$ and thus the resulting friction work W (Eq. (1)) and mean surface heat flux $\bar{\varphi}$ (Eq. (2), based on [47–49]) generated at the contact interface are close for the three configurations (cCo, cCu, and cNC). The terms F_T, L_S, and S are respectively the friction force, the sliding distance, and the apparent contact area. The Taylor-Quinney coefficient β_{TQ} represents the fraction of the friction work (or surface power $P = \mu.p.v$) dissipated as heat (or surface heat flux φ). As it is usually in the 0.9-1 range, a value of 0.95 was used for numerical applications.

$$W = F_T.L_S = \underline{\mu}.p.S.L_S \tag{1}$$

$$\bar{\varphi} = \beta_{TQ}.P = \beta_{TQ}.\underline{\mu}.p.v \tag{2}$$

The coating material effect on the tribological behavior is evaluated through the thickness of the heat affected and sheared zones in the slider as this part is made of the same material in both configurations. For cCo and cCu, both results are presented in Section 3.2. For cNC, the results come from Chassaing's work [39].

The behavior scenario presented in Section 3.4 considers that the third body is quickly generated and then lubricates the downstream contact (the "wet" part), decreasing the local friction coefficient. Conversely, it means that most of the friction work is dissipated in the part of the contact without third body (the "dry" part), called the active part of the contact. The active fraction of the contact is defined by the ratio R^{act} (see values in Tab. 1) of the active contact to the total contact areas and obtained via (Eq. (3)) from the deposit activation

length L^{act} (defined in Section 3.2). The cNC data [39] didn't include a SEM analysis of the surface. For that reason, L^{act} (7 mm) was determined from a longitudinal profile present in the reference.

$$R^{act} = \frac{L^{act}}{L_P} \tag{3}$$

The friction coefficient, and thus the shear stress, in the part of the contact protected by the third body are considered negligible. The contact pressure is supposed to be evenly distributed (over the whole contact area) and the friction coefficient to be constant in the active part of the contact. Consequently, an element of the surface of the slider is exposed for a duration $t^{act} = R^{act}.L_p/v$ to a shear stress τ^{act} and surface heat flux φ_s^{act} when going through the active part of the contact. Both are constant and calculated from R^{act} by using Eqs. (4) and (5) wherein k_s is the fraction of the surface heat flux dissipated toward the slider. Their values are reported in Tab. 1. In this configuration, both the shear stress τ^{act} and the surface heat flux are φ_s^{act} are inversely proportional to R^{act}. Conversely, the time t^{act} during which a point of the surface of the slider is exposed to these loads is proportional to R^{act}.

$$\tau^{act} = \frac{\underline{\mu}.p}{R^{act}} \tag{4}$$

$$\varphi_s^{act} = k_s.\frac{\underline{\varphi}}{R^{act}} \tag{5}$$

For the same macroscopic friction coefficient, the smaller the active part of the contact, (lower R^{act}), the higher the shear stresses predicted by the model are on the unprotected part of the contact. Higher shear stresses are coherent with the deeper sheared zone that had been observed for such coating.

Concerning the surface heat flux, it also evolves contrary to the size of the active part of the contact (Eq. (10)). However, unlike the surface heat flux, the heat affected depth increases with R^{act}. This phenomenon is linked to the decrease in the exposure time t^{act} cause by the reduction of R^{act}, illustrated by Fig. 14.

In its initial state, Ti6Al4V, which the slider is made of, contains both an α phase and a β one (see Section 2.2). In order for heat affectation by quenching to appear, two successive steps must take place. The α phase of the alloy must first transform into β phase (at a temperature above the β-transus of the alloy). It must then be quickly cooled in order for this phase to transform into a martensitic α' phase. If either of these steps does not occur, no quenching can take place.

The α→β transformation uses a diffusion mechanism and need time to take place. For example, reference [38] suggests to maintain Ti6Al4V for 0.1 to 1 hour at a temperature between 900 and 970°C before any quenching operation in order for the α→β transformation to occur. In the field of welding, Elmer et al. [50] highlighted the strong influence of heating speed on the temperature at which the α→β transformation occurred: "at a heating rate of 30°C/s, higher temperatures, on the order of 50°C, were required to produce the same amount of β phase as that predicted by equilibrium thermodynamics" [50]. To put these results into perspective, from the temperature evolution measured by Chassaing et al [30] in a test done in conditions close to the ones of the present paper ($v = 40$ m/s, and $p = 110$ MPa), mean heating rates of about 1,000,000°C/s are observed. We can infer that a temperature much higher than the β-transus is needed for the α→β transformation to occur.

Consequently, the longer a point of the surface of the slider is heated, the deeper under that point the α→β transformation will take place, which, after cooling, causes a deeper heat affected (quenched) zone to appear.

We see here that both the evolution of the sheared depth and the heat affected depth support the model proposed in Section 3.4. Given this analysis, further investigations into the severe contact between a non-coated Ti6Al4V slider and coated Ti6Al4V pads will have to link the thermomechanical properties of the first bodies to their microstructural alterations. This requires to know these properties, which proves to be, itself, a challenge. Furthermore, the

kinetic of the phase transformations (or lack thereof) in the materials involved is critical, especially when considering that said transformations may be influenced by the mechanical state (stress and strain) of the material. The effect of the third body on the evacuation of heat outside of the contact also needs to be studied. As it is evacuated from the contact at high temperature, it may behave like grinding chips and absorb a significant part of the heat resulting from the friction [51]. Finally, given the small range of usual values of the Taylor-Quinney coefficient (0.9 to 1), it is not necessary to focus on its determination for now.

4 Conclusions

Couples of a Ti6Al4V slider and a Ti6Al4V pad, coated of either CuNiIn or CoCrAlYSiBN were subjected to friction experiments on a slider-on-pad tribometer. Under an apparent contact pressure of 110 or 280 MPa, initial sliding speeds ranging between 36 and 68 m/s were quasi-instantaneously applied to the slider. From the tests, the friction coefficient, wear volume and microstructural alterations were investigated and compared to the results from tests with non-coated pads.

The following conclusions were drawn:

1. The coating integrity was preserved with both CoCrAlYSiBN and CuNiIn materials, with no severe wear mode (e.g. spalling or delamination) being observed.
2. At a macroscopic scale (friction coefficient and pad wear), the use of both coatings led to similar results. When compared to an absence of coating, they reduced pad wear while not significantly changing the friction coefficient.
3. The friction coefficient and wear of the coated pads presented little to no sensibility to the sliding speed but were influenced by the apparent contact pressure. Increasing the apparent contact pressure from 110 to 280 MPa halved the friction coefficient and increased wear by up to about 1 mm^3.

4. A behavior scenario was proposed for contacts in severe friction with interface-localized heat. Based on the microstructural layering of the slider, it is time-independent and position-dependent, following an element of the slider surface.
5. The thicknesses of the heat-affected and sheared layers (of the slider) were dependent on the coating used. This was shown to be linked to a difference in the active (non-lubricated by the third body) length of the contact which we proposed to at least be dependent on the thermal properties of the components and on their thermomechanical behavior.
6. At $v = 40$ m/s and $p = 280$ MPa, the CuNiIn coating was more easily worn than the CoCrAlYSiBN one, facilitating the formation of the third body and therefore slightly reducing the friction coefficient.

Acknowledgements:

We would like to sincerely thank the editor and the three reviewers for their helpful comments which helped to improve the quality of this paper since it was first submitted. We would also like to thank Marjorie Antoni for proofreading our manuscript.

Funding:

This work was supported by IRT M2P, Metz, France.

Conflict of interest:

None.

References

[1] Combres Y. Propriétés du titane et de ses alliages. Tech l'Ingénieur 1999;33.

[2] Boyer RR. An overview on the use of titanium in the aerospace industry. Mater Sci Eng A 1996;213:103–14. doi:10.1016/0921-5093(96)10233-1.

[3] Budinski KG. Tribological properties of titanium alloys. Wear 1991;151:203–17. doi:http://dx.doi.org/10.1016/0043-1648(91)90249-T.

[4] Fayeulle S, Blanchard P, Vincent L. Fretting Behavior of Titanium Alloys. Tribol Trans 1993;36:267–75. doi:10.1080/10402009308983158.

[5] Long M, Rack HJ. Friction and surface behavior of selected titanium alloys during reciprocating-sliding motion. Wear 2001;249:157–67. doi:10.1016/S0043-1648(01)00517-8.

[6] Barman K, Shipway PH, Voisey KT, Pattinson G. The role of a thermally sprayed CuNiIn underlayer in the durability of a dry-film lubricant system in fretting – A phenomenological model. Tribol Int 2018;123:307–15. doi:https://doi.org/10.1016/j.triboint.2018.03.018.

[7] Kim K, Korsunsky AM. Dissipated energy and fretting damage in CoCrAlY-MoS2 coatings. Tribol Int 2010;43:676–84. doi:https://doi.org/10.1016/j.triboint.2009.10.007.

[8] Hajmrle K, Chilkowich AP. Low friction cobalt based coatings for titanium alloys. US 5601933 A, 1997.

[9] Freimanis AJ, Segall AE, Conway JCJ, Whitney EJ. The Influence of Temperature on the Wear Mode and Deterioration of Coatings Used For Titanium Aircraft Engine Components. Tribol Trans 2002;45:193–8. doi:10.1080/10402000208982539.

[10] Fridrici V, Fouvry S, Kapsa P. Fretting wear behavior of a Cu–Ni–In plasma coating. Surf Coatings Technol 2003;163:429–34. doi:10.1016/S0257-8972(02)00639-4.

[11] Rajasekaran B, Raman SGS, Joshi S V., Sundararajan G. Performance of plasma sprayed and detonation gun sprayed Cu–Ni–In coatings on Ti–6Al–4V under plain fatigue and fretting fatigue loading. Mater Sci Eng A 2008;479:83–92. doi:10.1016/j.msea.2007.06.019.

[12] Lim SC, Ashby MF, Brunton JH. The effects of sliding conditions on the dry friction of metals. Acta Metall 1989;37:767–72. doi:http://dx.doi.org/10.1016/0001-6160(89)90003-5.

[13] Bowden FP, Tabor D. The Area of Contact between Stationary and between Moving Surfaces. Proc R Soc London Ser A Math Phys Sci 1939;169:391 LP-413.

[14] Bowden FP, Thomas FH. The surface temperature of sliding solids. Proc R Soc London Ser A Math Phys Sci 1954;223:29 LP-40.

[15] Archard JF. The temperature of rubbing surfaces. Wear 1959;2:438–55. doi:https://doi.org/10.1016/0043-1648(59)90159-0.

[16] Archard JF, Rowntree RA. The temperature of rubbing bodies; part 2, the distribution of temperatures. Wear 1988;128:1–17. doi:https://doi.org/10.1016/0043-1648(88)90249-9.

[17] Molinari A, Estrin Y, Mercier S. Dependence of the Coefficient of Friction on the Sliding Conditions in the High Velocity Range. J Tribol 1999;121:35–41. doi:10.1115/1.2833808.

[18] Kimball AS. A new investigation of one of the laws of friction. Am J Sci 1877.

[19] Bowden FP, Freitag EH. The Friction of Solids at Very High Speeds. I. Metal on Metal; II. Metal on Diamond. Proc R Soc London A Math Phys Eng Sci 1958;248:350–67.

[20] Bowden FP, Persson PA. Deformation, Heating and Melting of Solids in High-Speed Friction. Proc R Soc London A Math Phys Eng Sci 1961;260:433–58.

[21] Montgomery RS. Friction and wear at high sliding speeds. Wear 1976;36:275–98. doi:http://dx.doi.org/10.1016/0043-1648(76)90108-3.

[22] Prakash V. A pressure-shear plate impact experiment for investigating transient friction. Exp Mech 1995;35:329–36. doi:10.1007/BF02317542.

[23] Philippon S, Sutter G, Molinari A. An experimental study of friction at high sliding velocities. Wear 2003;257:777–84. doi:10.1016/j.wear.2004.03.017.

[24] Lodygowski A, Voyiadjis GZ, Deliktas B, Palazotto A. Non-local and numerical formulations for dry sliding friction and wear at high velocities. Int J Plast 2011;27:1004–24. doi:10.1016/j.ijplas.2010.10.008.

[25] Uetz H, Föhl J. Wear as an energy transformation process. Wear 1978;49:253–64. doi:http://dx.doi.org/10.1016/0043-1648(78)90091-1.

[26] Rigney DA, Hirth JP. Plastic deformation and sliding friction of metals. Wear 1979;53:345–70. doi:10.1016/0043-1648(79)90087-5.

[27] Landman U, Luedtke WD, Ringer EM. Molecular dynamics simulations of adhesive contact formation and friction. Kluwer Academic; 1992.

[28] Kennedy FE. Single Pass Rub Phenomena—Analysis and Experiment. J Lubr Technol 1982;104:582–8.

[29] Bowden FP, Ridler KEW. A Note on the Surface Temperature of Sliding Metals. Math Proc Cambridge Philos Soc 1935;31:431–2. doi:DOI: 10.1017/S0305004100077501.

[30] Chassaing G, Pougis A, Philippon S, Lipinski P, Faure L, Meriaux J, et al. Experimental and numerical study of frictional heating during rapid interactions of a Ti6Al4V tribopair. Wear 2015;342:322–33. doi:10.1016/j.wear.2015.09.013.

[31] Qiu M, Zhang Y-Z, Shangguan B, Du S-M, Yan Z-W. The relationships between tribological behaviour and heat-transfer capability of Ti6Al4V alloys. Wear 2007;263:653–7. doi:10.1016/j.wear.2006.12.041.

[32] Qiu M, Zhang Y, Zhu J, Yang J. Dry friction characteristics of Ti-6Al-4V alloy under high sliding velocity. J Wuhan Univ Technol Sci Ed 2007;22:582–5. doi:10.1007/s11595-006-4582-0.

[33] Faure L, Bolle B, Philippon S, Schuman C, Chevrier P, Tidu a. Friction Experiments for titanium alloy tribopairs sliding in dry conditions: Sub-surface and surface analysis. Tribol Int 2012;54:17–25. doi:10.1016/j.triboint.2012.04.007.

[34] Chassaing G, Faure L, Philippon S, Coulibaly M, Tidu A, Chevrier P, et al. Adhesive wear of a Ti6Al4V tribopair for a fast friction contact. Wear 2014;320:25–33. doi:10.1016/j.wear.2014.08.001.

[35] Lim SC, Ashby MF. Overview no. 55 Wear-Mechanism maps. Acta Metall 1987;35:1–24. doi:10.1016/0001-6160(87)90209-4.

[36] Elmer JW, Palmer TA, Babu SS, Zhang W, DebRoy T. Phase transformation dynamics

during welding of Ti–6Al–4V. J Appl Phys 2004;95:8327–39. doi:10.1063/1.1737476.

[37] Welsch G, Boyer R, Collings EW. Materials properties handbook: titanium alloys. ASM international; 1993.

[38] Combres Y, Champin B. Traitements thermiques des alliages de titane. Tech l'Ingénieur 2013;33.

[39] Chassaing G. Frottement sec à grande vitesse du couple Ti6Al4V-Ti6Al4V : étude expérimentale et modélisation du comportement thermomécanique. Université de Lorraine, 2015.

[40] Gowda BMA, Yeshovanth HR, Siddaraju C. Investigation and Efficient Modeling of an Dovetail Attachment in Aero-engine. Procedia Mater Sci 2014;5:1873–9. doi:http://dx.doi.org/10.1016/j.mspro.2014.07.495.

[41] Ogawa K. Impact friction test method by applying stress wave. Exp Mech 1997;37:398–402. doi:10.1007/BF02317304.

[42] Philippon S. Etude expérimentale du frottement sec à grandes vitesses de glissement. Université de Metz, 2004.

[43] Chassaing G, Pougis A, Philippon S, Lipinski P, Meriaux J, Faure L. Initiation of Adhesive Wear During Frictional Interaction at Very High Velocity for a Ti6Al4V Tribopair. Proc. 13th World Conf. Titan., 2016, p. 5–7. doi:10.1002/9781119296126.ch274.

[44] Bahr H-A, Fischer G, Weiss H-J. Thermal-shock crack patterns explained by single and multiple crack propagation. J Mater Sci 1986;21:2716–20. doi:10.1007/BF00551478.

[45] Godet M. Third-bodies in tribology. Wear 1990;136:29–45. doi:https://doi.org/10.1016/0043-1648(90)90070-Q.

[46] Denape J, Berthier Y, Vincent L. Wear Particle Life in a Sliding Contact Under Dry Conditions : Third Body Approach BT - Fundamentals of Tribology and Bridging the Gap Between the Macro- and Micro/Nanoscales. In: Bhushan B, editor. Fundam. Tribol. Bridg. Gap Between Macro- Micro/Nanoscales, Dordrecht: Springer Netherlands; 2001, p. 393–411. doi:10.1007/978-94-010-0736-8_28.

[47] Earles SWE, Powell DG. Surface Temperature and Its Relation to Periodic Changes in Sliding Conditions between Unlubricated Steel Surfaces. A S L E Trans 1968;11:109–20. doi:10.1080/05698196808972214.

[48] Coulibaly M, Chassaing G, Philippon S. Thermomechanical coupling of rough contact asperities sliding at very high velocity. Tribol Int 2014;77:86–96. doi:10.1016/j.triboint.2014.04.014.

[49] Kennedy FE. Frictional heating and contact temperatures. In: Bhushan B, Kennedy FE, Szeri AZ, editors. Mod. Tribol. Handb., CRC Press; 2000, p. 235–72.

[50] Elmer JW, Palmer TA, Babu SS, Specht ED. In situ observations of lattice expansion and transformation rates of α and β phases in Ti–6Al–4V. Mater Sci Eng A 2005;391:104–13. doi:https://doi.org/10.1016/j.msea.2004.08.084.

[51] Fritz Klocke E h., Kuchie A. Grinding, 2009, p. 1–166. doi:10.1007/978-3-540-92259-9_6.

List of figures

Figure number	Caption	Suggested width
1	Samples configuration	1 column
2	Typical recording (test of Ti6Al4V against Ti6Al4V+CoCrAlYSiBN at $v = 40$ m/s and $p = 110$ MPa)	1 column
3	Initial microstructure of the materials	1,5 columns
4	Microstructural observation positions	1 column
5	Friction coefficient $\bar{\mu}$ as a function of the sliding speed	1 column
6	Apparent wear volume w as a function of the sliding speed	1 column
7	Typical coated pad surface after experiment	1,5 columns
8	Repartition of the deposited layer at the surface of the pad (example of cCu)	1 column
9	Typical slider surface after experiment	1 column
10	EDX spectrum of the deposited layer in the cCu and cCo configurations ($v = 40$ m/s and $p = 110$ MPa)	1 column
11	Typical samples microstructure after experiment	2 columns
12	Microstructure of the layer deposited on the pad	1 column
13	Behavior scenario of the Ti6Al4V-Ti6Al4V+Coating contacts	1,5 columns
14	Third body influence on the heat affectation of the slider	1 column

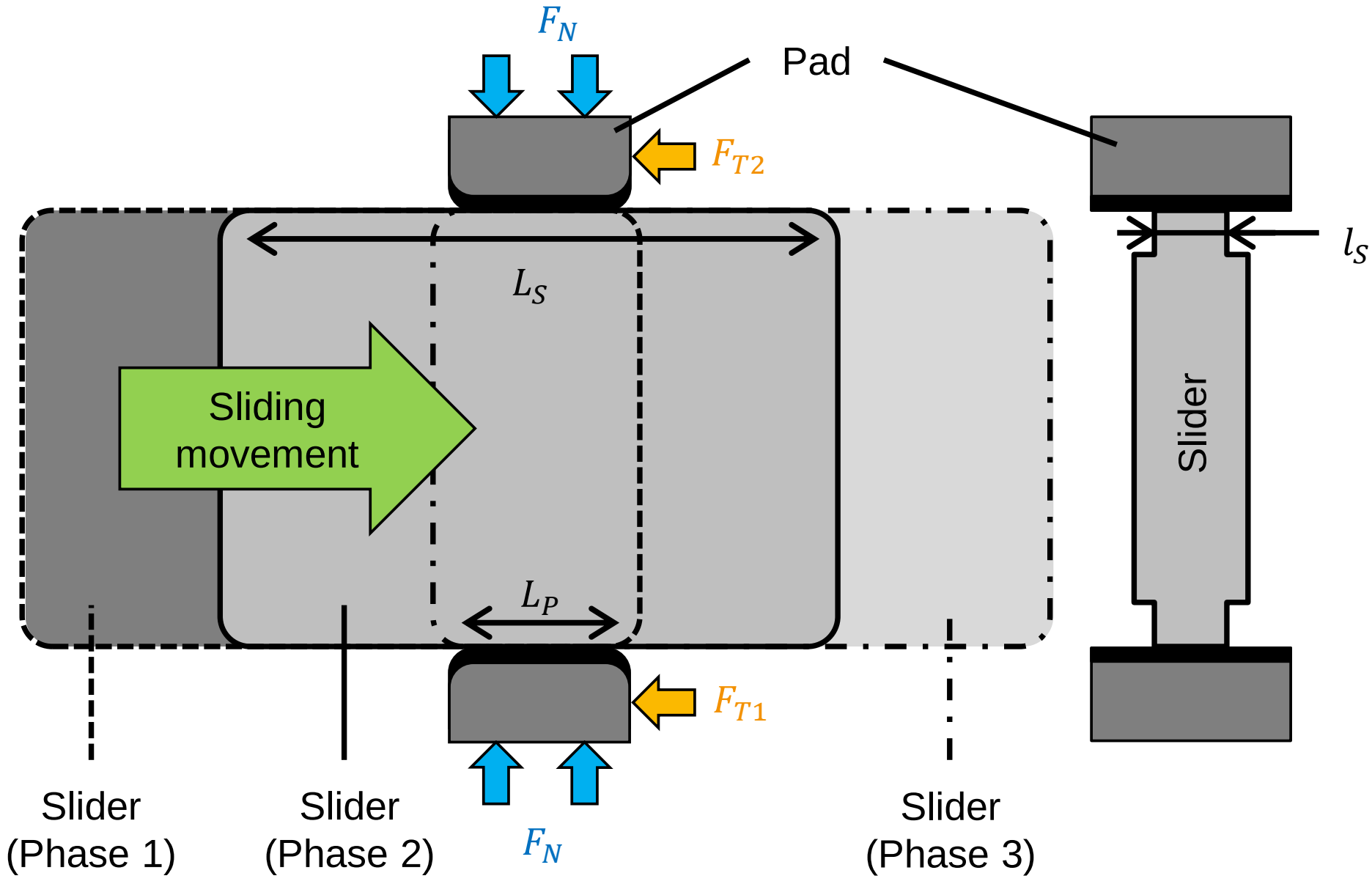
F_N
Pad
F_{T2}
l_S
L_S
Sliding movement
Slider
L_P
F_{T1}
Slider (Phase 1)
Slider (Phase 2)
F_N
Slider (Phase 3)

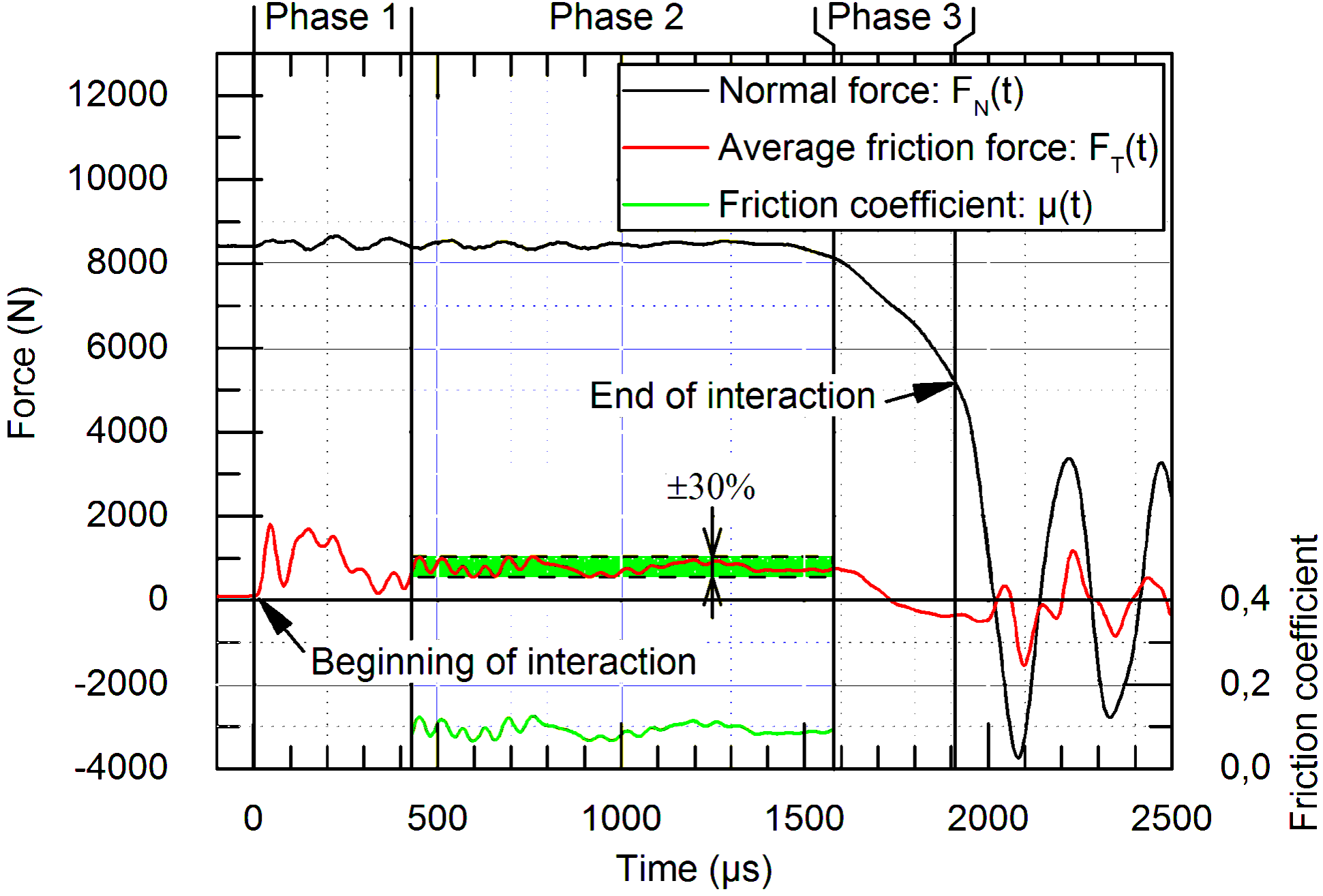
Phase 1
Phase 2
Phase 3
Normal force: $F_N(t)$
Average friction force: $F_T(t)$
Friction coefficient: μ(t)
End of interaction
±30%
Beginning of interaction
Force (N)
12000
10000
8000
6000
4000
2000
0
-2000
-4000
0
500
1000
1500
2000
2500
Time (μs)
0,4
0,2
0,0
Friction coefficient

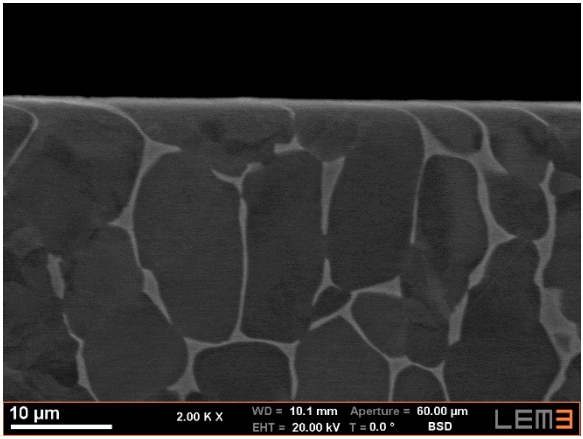

a. Ti6Al4V

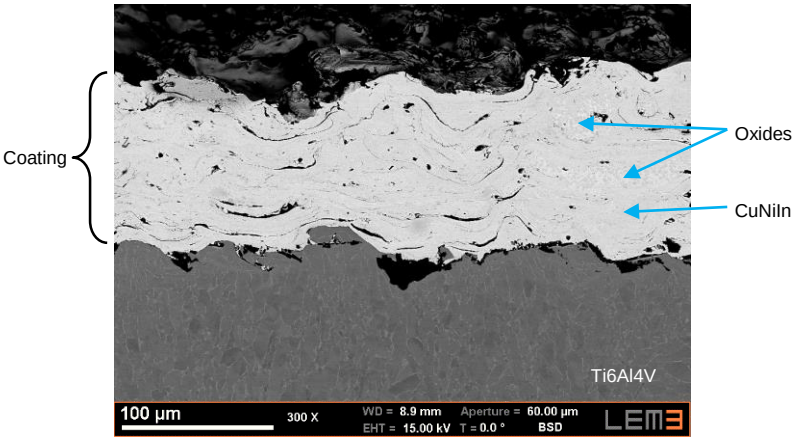

b. CuNiIn

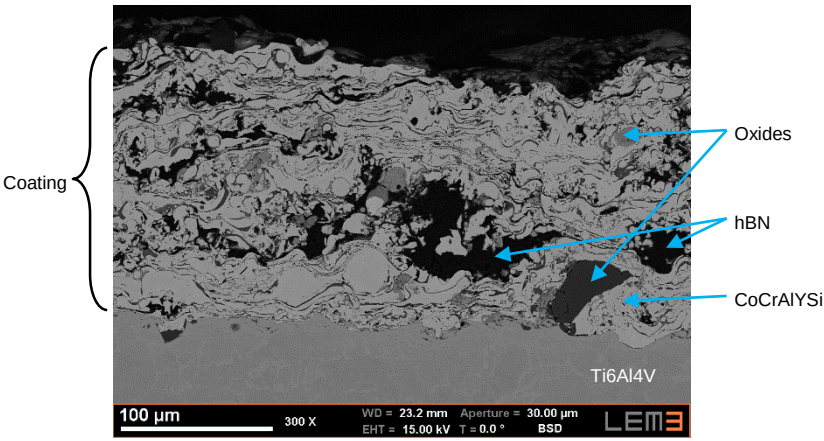

c. CoCrAlYSiBN

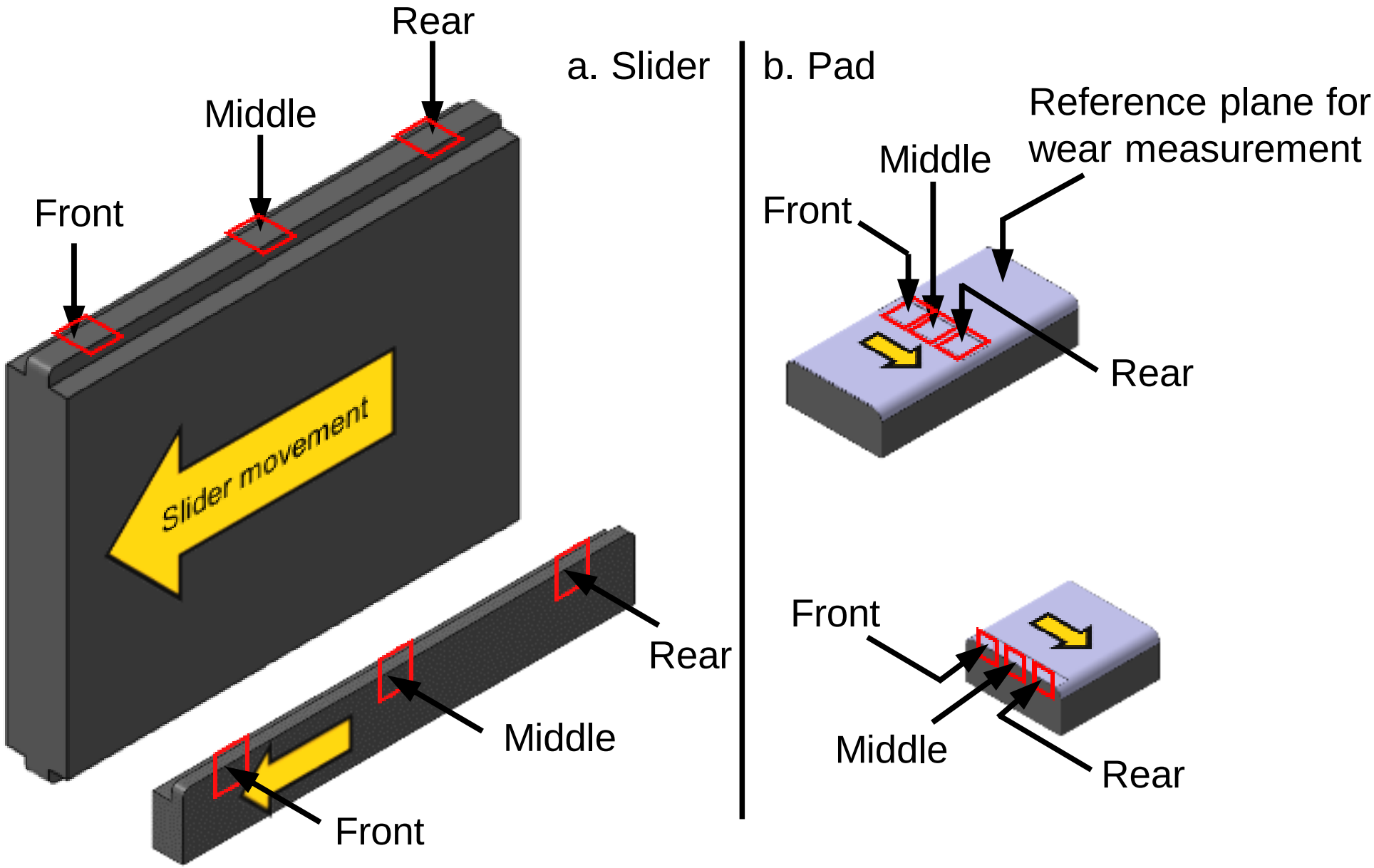
Rear
Middle
Front
Slider movement
Rear
Middle
Front
a. Slider
b. Pad
Reference plane for wear measurement
Middle
Front
Rear
Front
Middle
Rear

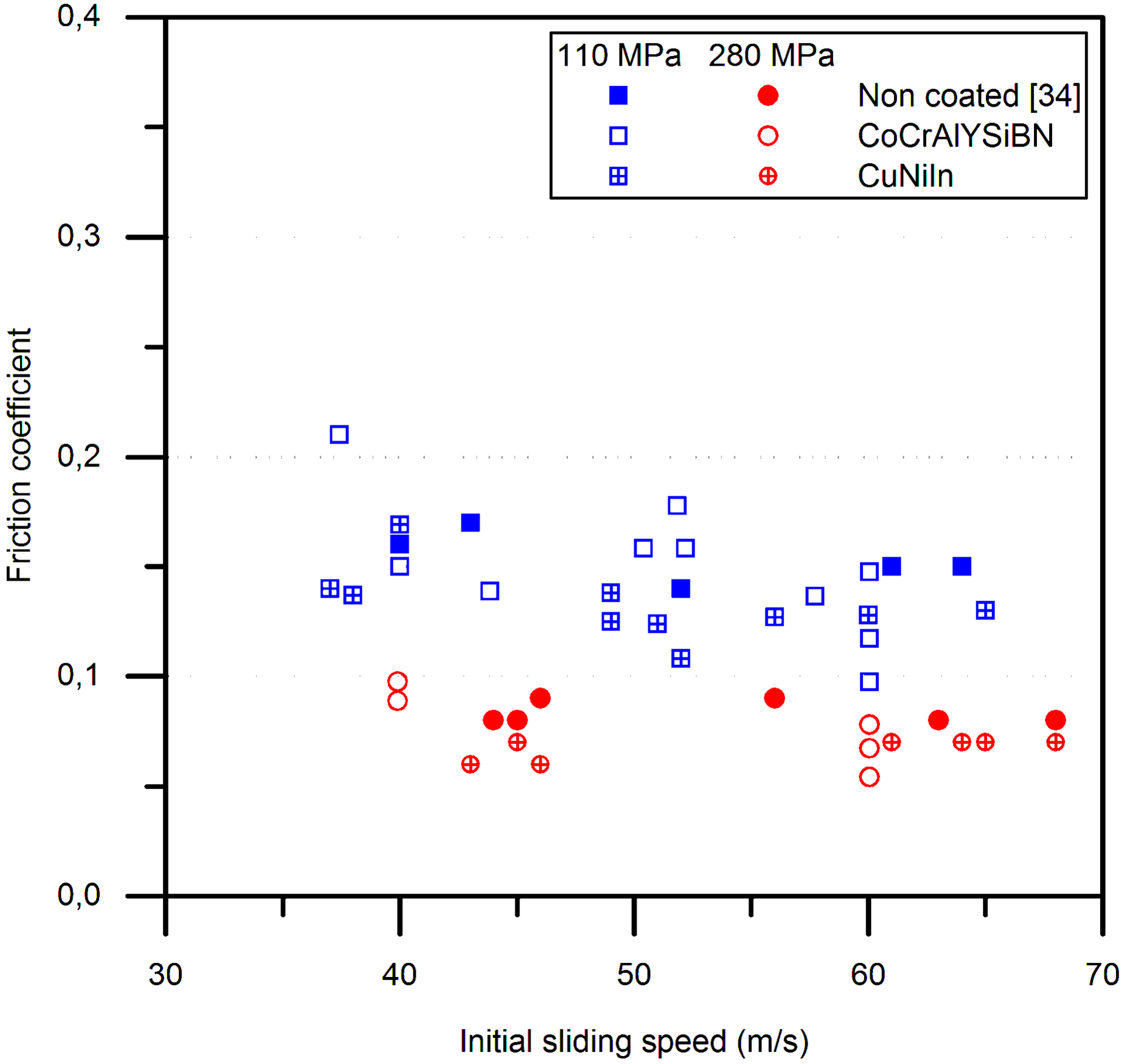
110 MPa
280 MPa
Non coated [34]
CoCrAlYSiBN
CuNiIn
Friction coefficient
0,0
0,1
0,2
0,3
0,4
30
40
50
60
70
Initial sliding speed (m/s)

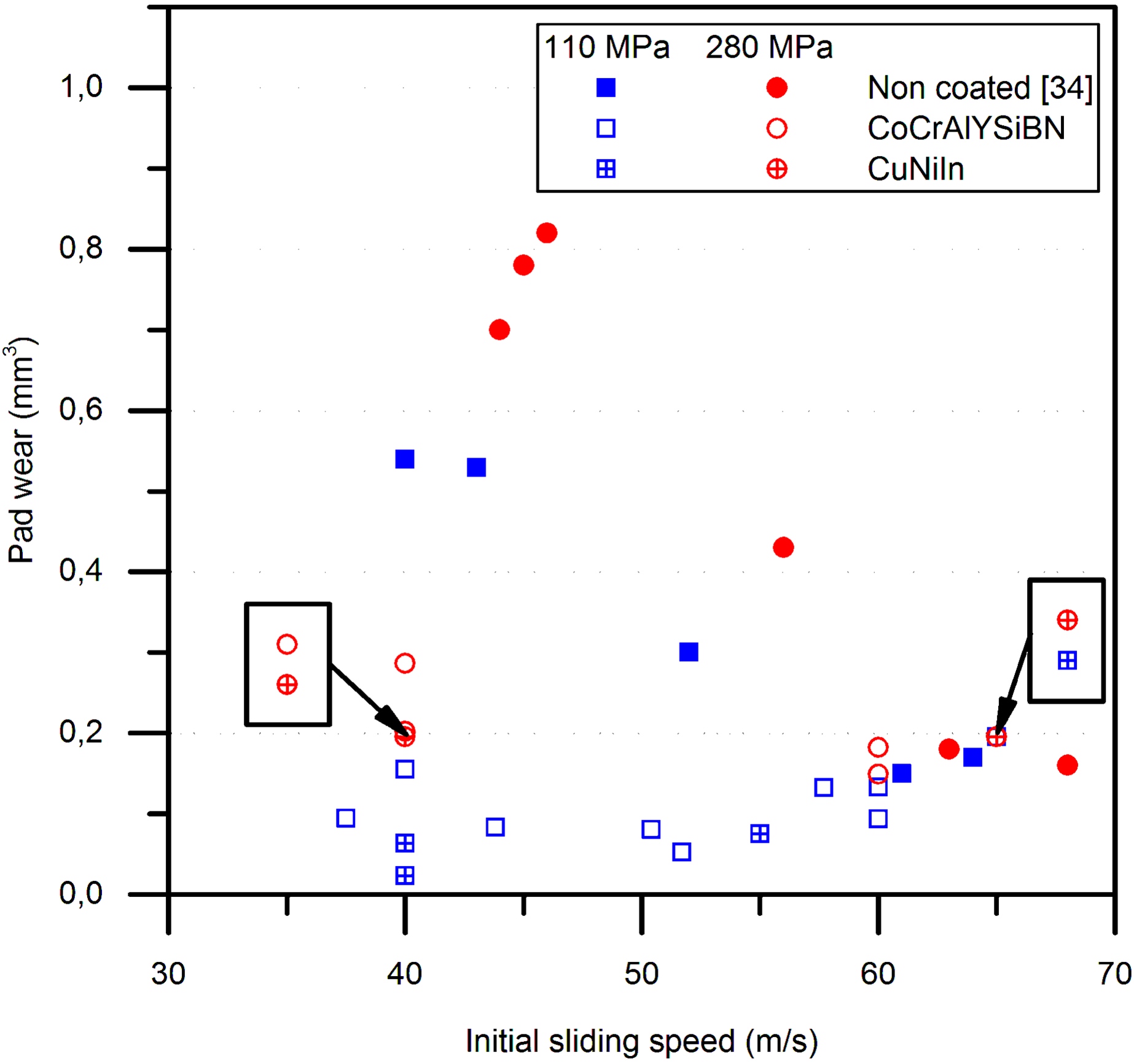
110 MPa
280 MPa
Non coated [34]
CoCrAlYSiBN
CuNiIn
Pad wear (mm3)
1,0
0,8
0,6
0,4
0,2
0,0
30
40
50
60
70
Initial sliding speed (m/s)

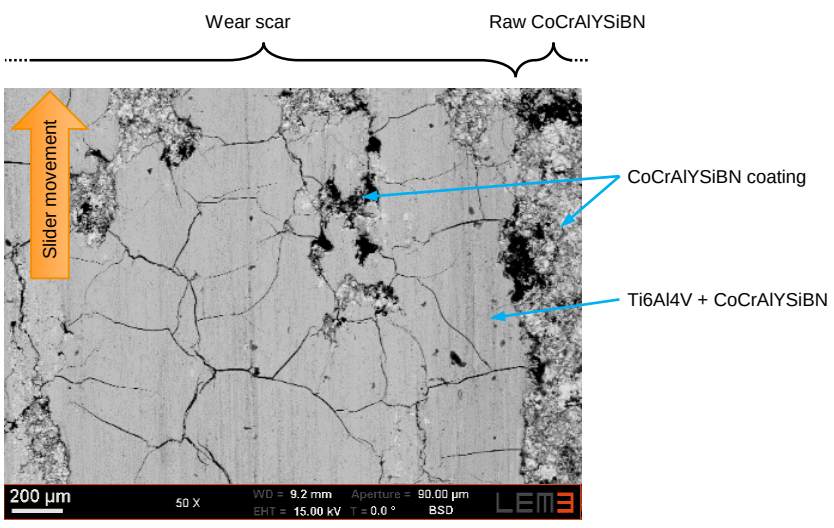

a. CoCrAlYSiBN

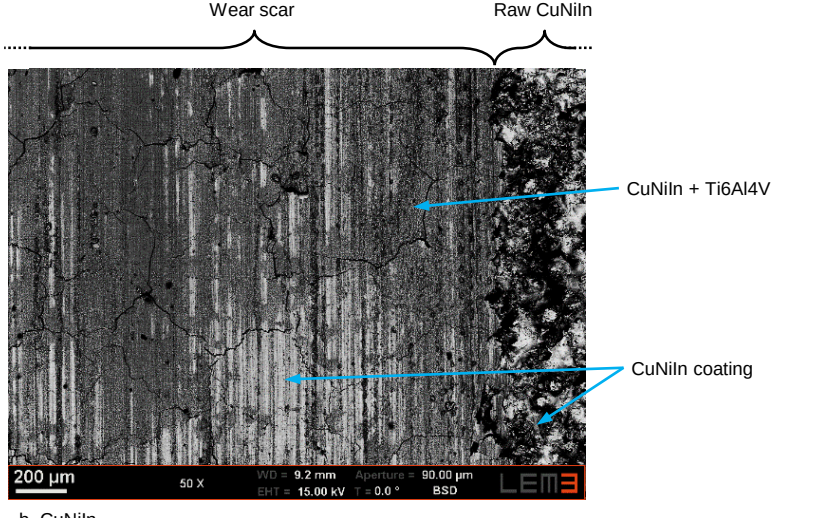

b. CuNiIn

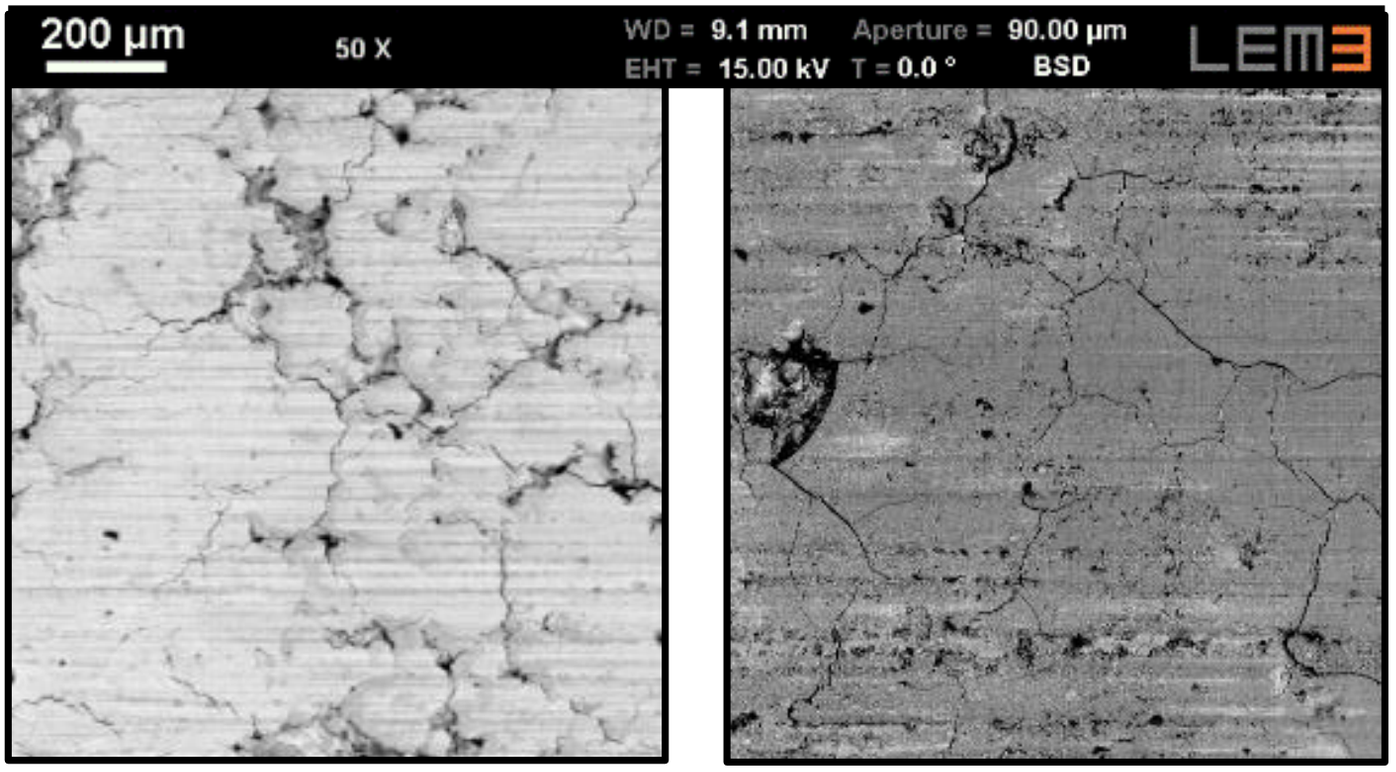

No deposit

Deposit

Friction scar

Slider movement

L^{act}

L_P

Front edge

Back edge

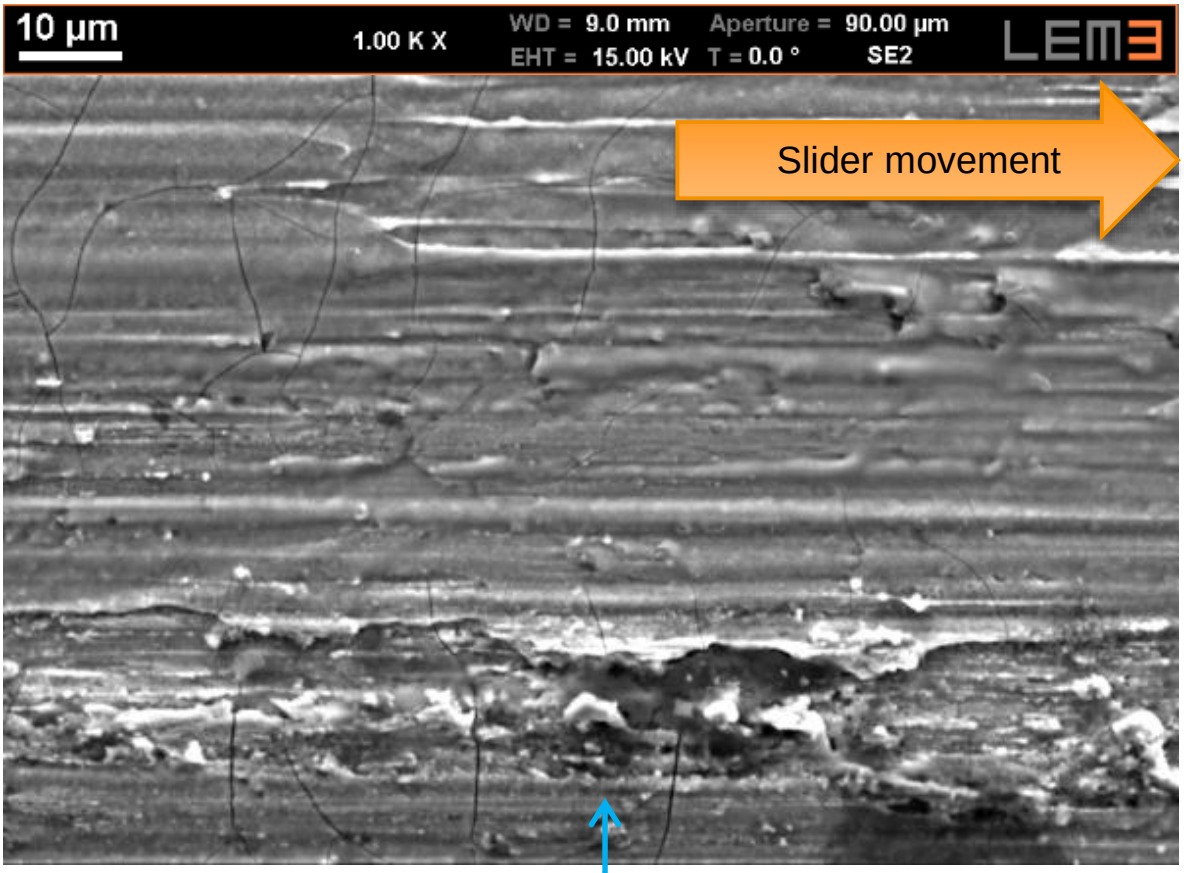

a. CoCrAlYSiBN

Ti6Al4V slider

Third body deposit

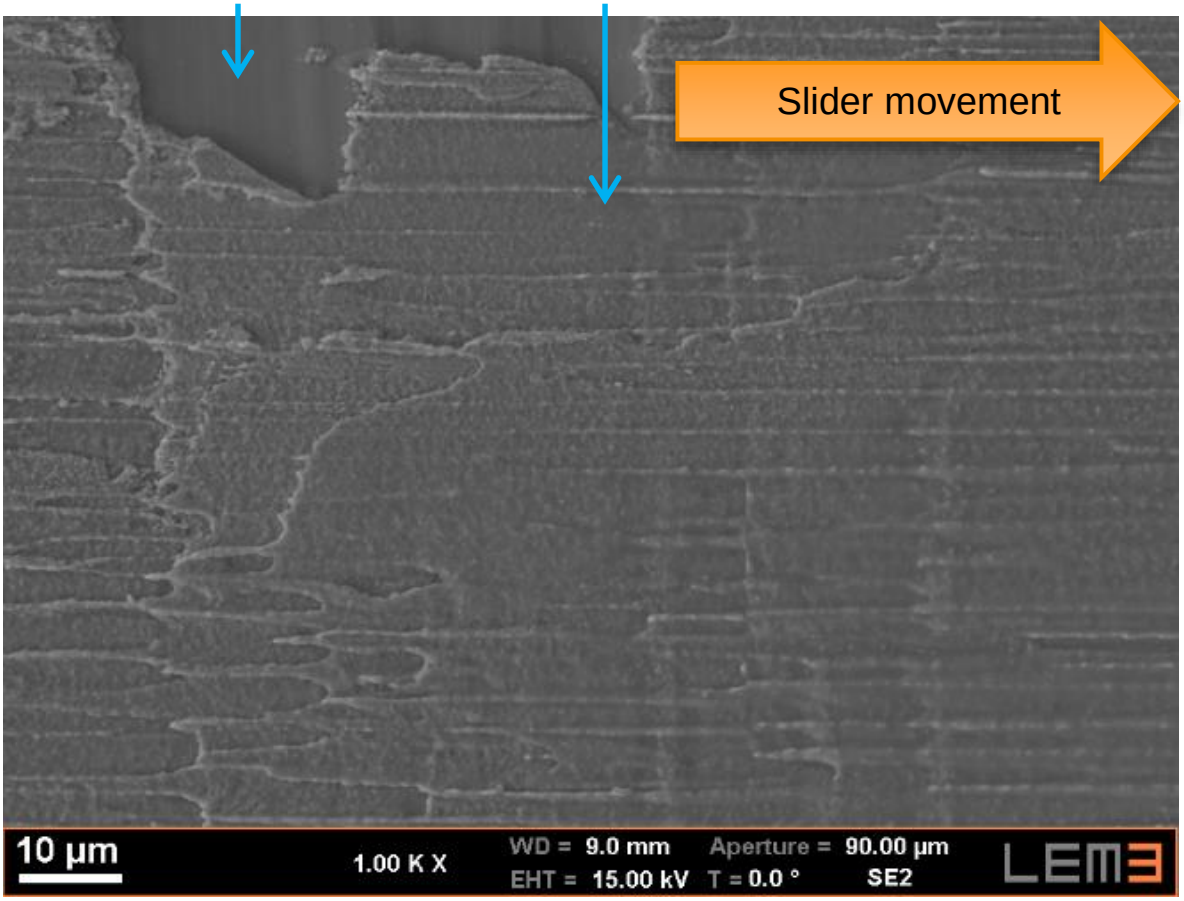

b. CuNiIn

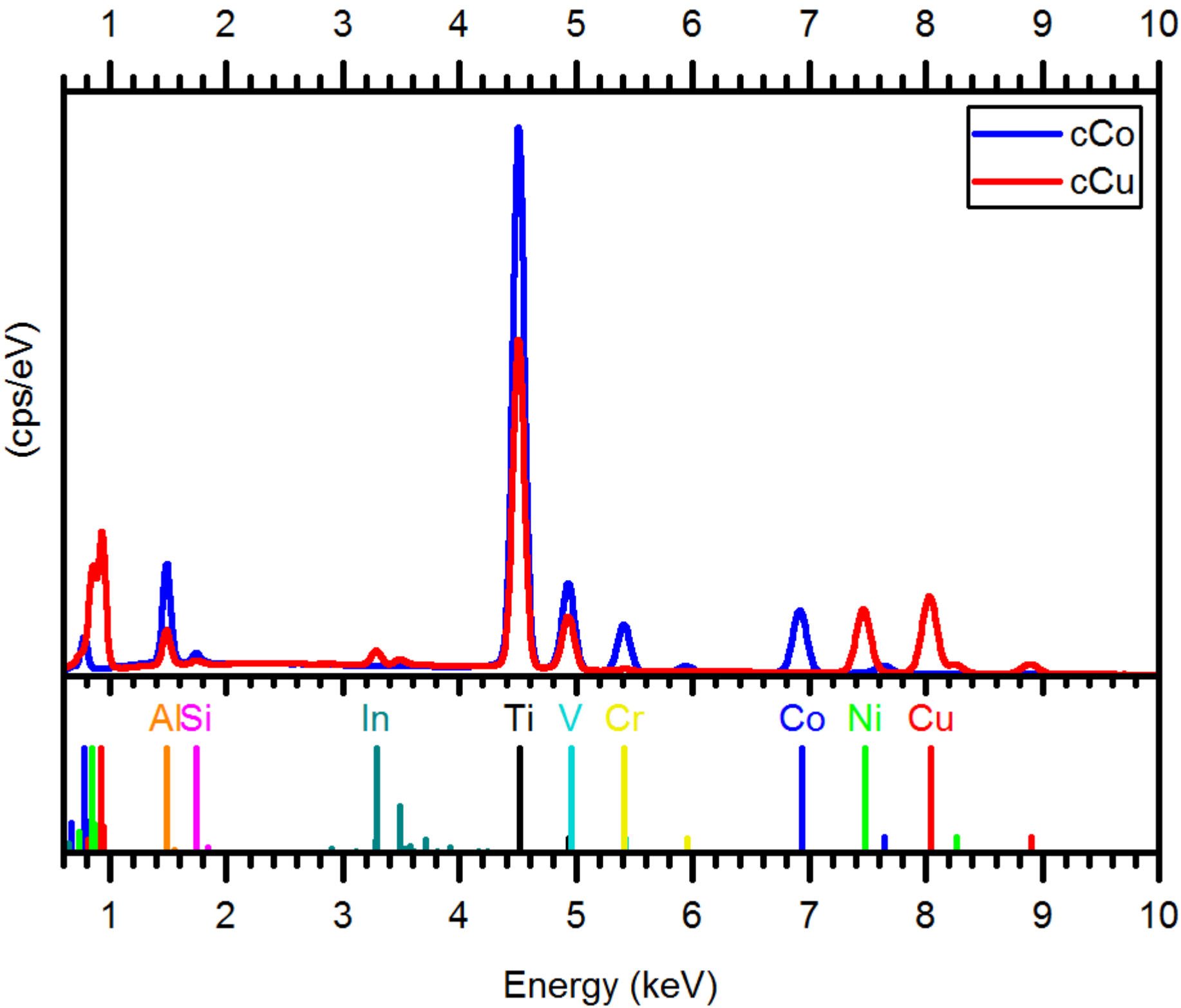
cCo
cCu
(cps/eV)
Al
Si
In
Ti
V
Cr
Co
Ni
Cu
Energy (keV)

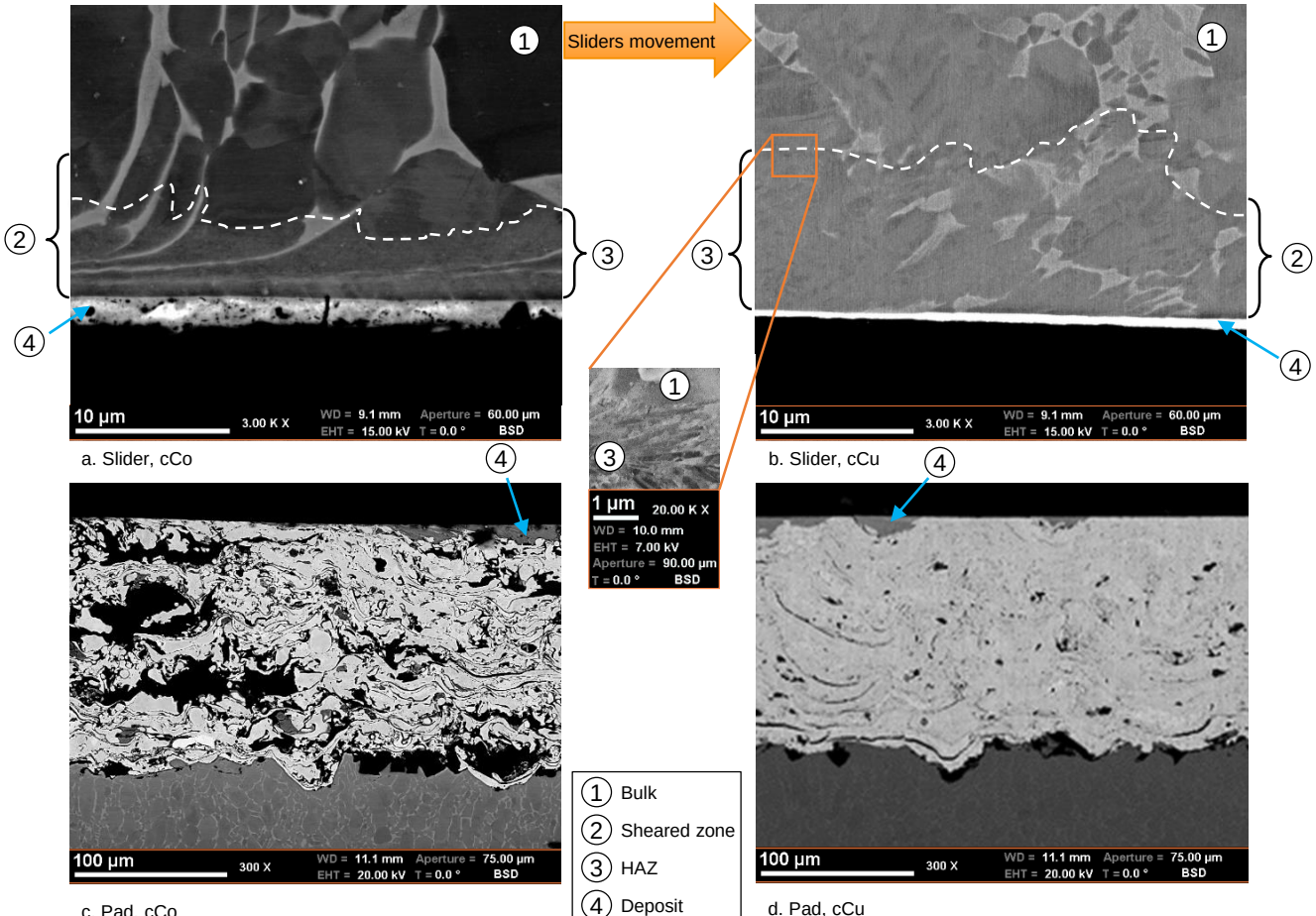
Sliders movement
1
2
3
4
10 µm
3.00 K X
WD = 9.1 mm
Aperture = 60.00 µm
EHT = 15.00 kV
T = 0.0 °
BSD
a. Slider, cCo
b. Slider, cCu
1 µm
20.00 K X
WD = 10.0 mm
EHT = 7.00 kV
Aperture = 90.00 µm
T = 0.0 °
BSD
100 µm
300 X
WD = 11.1 mm
Aperture = 75.00 µm
EHT = 20.00 kV
T = 0.0 °
BSD
c. Pad, cCo
d. Pad, cCu
1 Bulk
2 Sheared zone
3 HAZ
4 Deposit

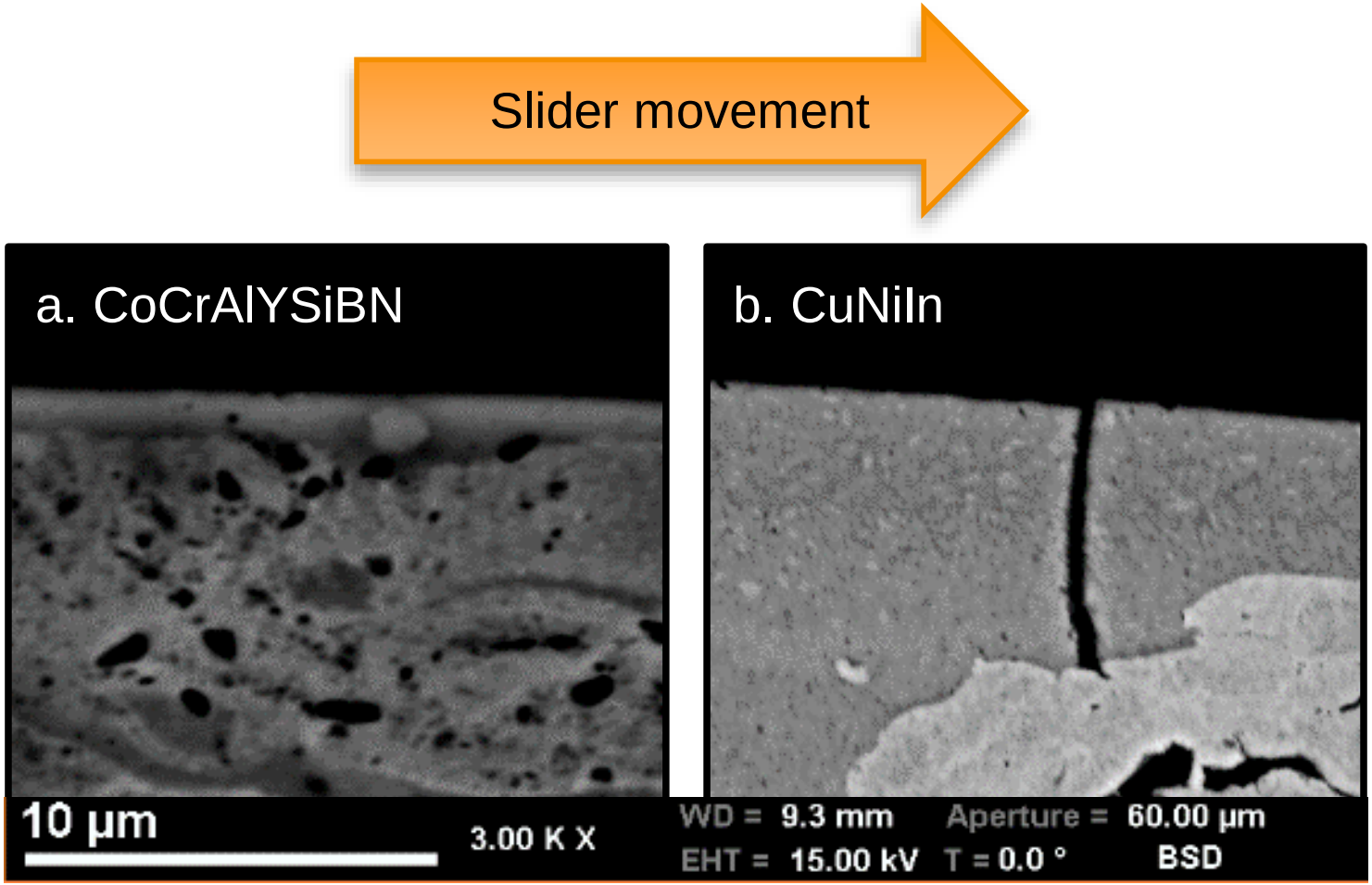
Slider movement
a. CoCrAlYSiBN
b. CuNiIn
10 µm
3.00 K X
WD = 9.3 mm
Aperture = 60.00 µm
EHT = 15.00 kV
T = 0.0 °
BSD

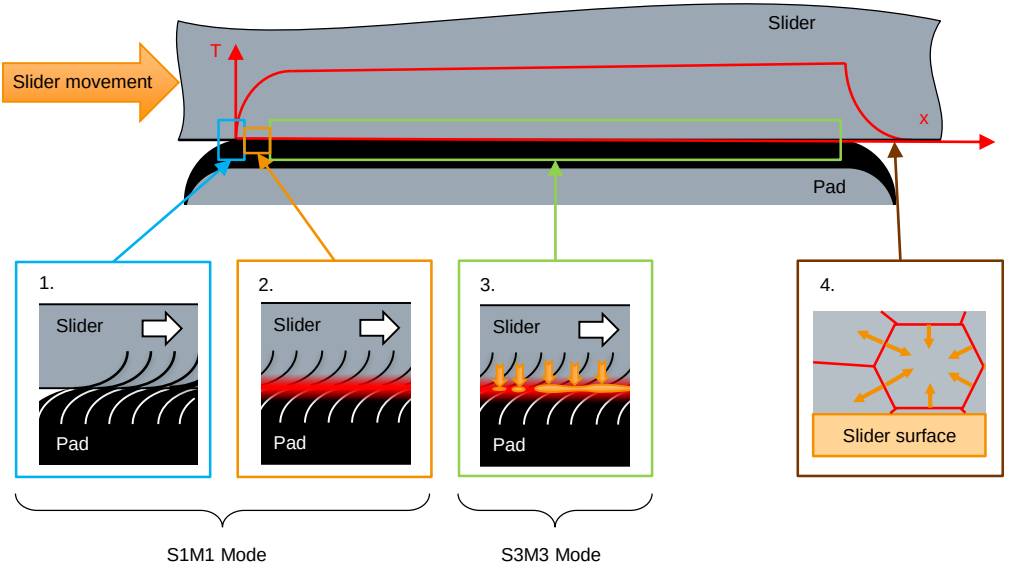
Slider movement
T
Slider
x
Pad
1.
Slider
Pad
2.
Slider
Pad
3.
Slider
Pad
4.
Slider surface
S1M1 Mode
S3M3 Mode

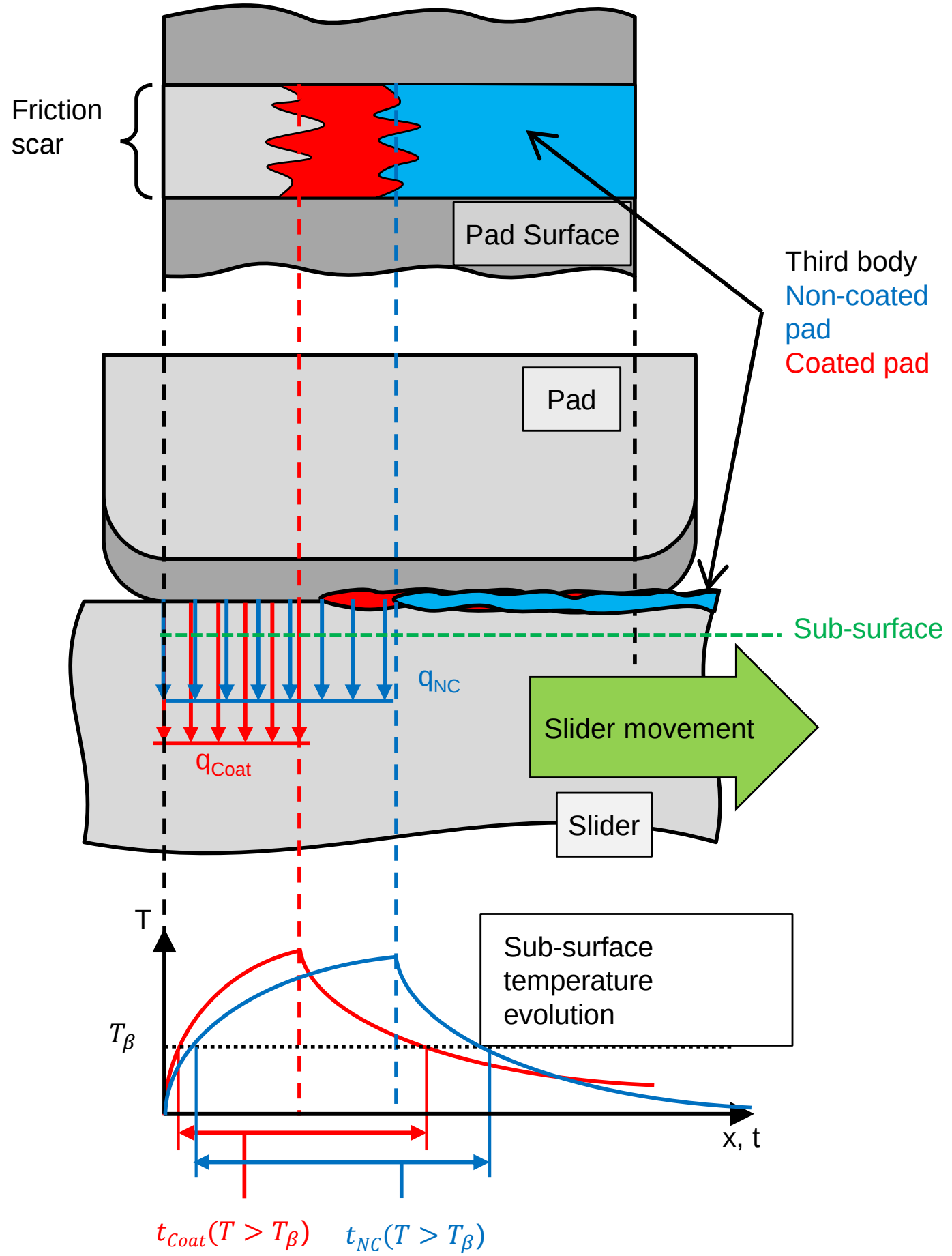
Friction scar
Pad Surface
Third body
Non-coated pad
Coated pad
Pad
Sub-surface
q_{NC}
q_{Coat}
Slider movement
Slider
T
T_β
Sub-surface temperature evolution
x, t
$t_{Coat}(T > T_\beta)$
$t_{NC}(T > T_\beta)$

1. Comparison of the three configurations for a test at v=40 m/s and p=110 MPa

		Pad surface material		
		CoCrAlYSiBN	CuNiIn	Ti6Al4V [44]
Typical microstructural alterations of the slider				
Micrograph layering ① Bulk ② Sheared zone ③ Heat affected zone ④ Third body deposit Slider movement 10 µm		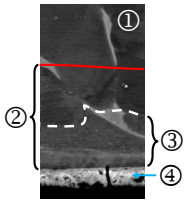	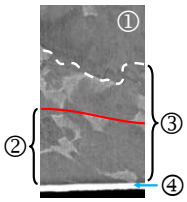	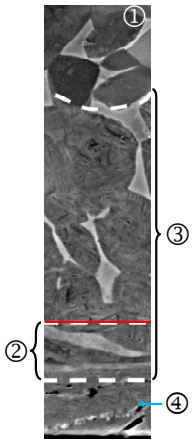
Heat affected depth	[µm]	5-10	10	20-30
Sheared depth	[µm]	10	5-7	5
Macroscopic results				
Friction coefficient $\overline{\mu}$		0.16	0.15	0.17
Total friction work W	[J]	32	30	34
Mean surface heat flux $\overline{\varphi}$	[W/mm²]	669	627	710
Results for the active part of the contact, according to Eqs. (3)-(5)				
Active fraction of the contact area R^{act}		20-30%	50%	70%
Friction stress τ^{act}	[MPa]	70	33	27
Surface heat flux φ^{act}	[W/mm²]	2534	1320	1070

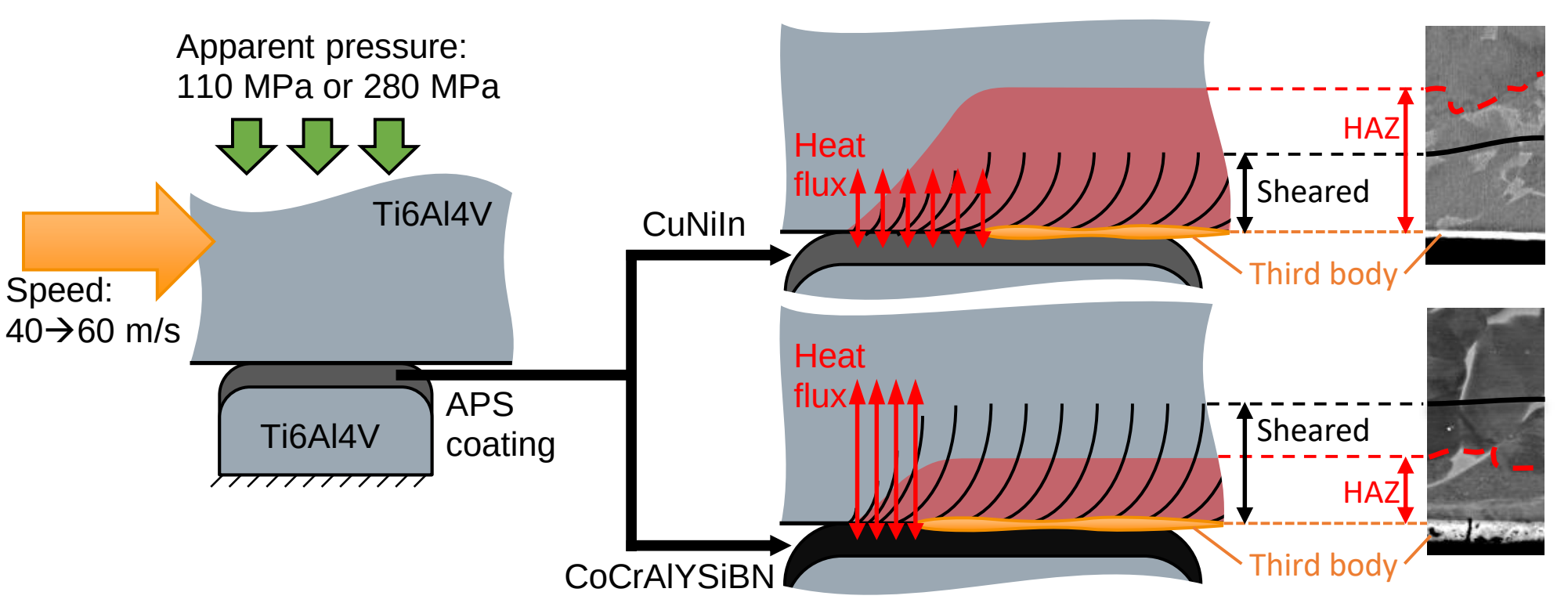
Apparent pressure:
110 MPa or 280 MPa
Ti6Al4V
Speed:
40→60 m/s
Ti6Al4V
APS
coating
CuNiIn
CoCrAlYSiBN
Heat
flux
Heat
flux
HAZ
Sheared
Third body
Sheared
HAZ
Third body